

PCCP

Accepted Manuscript



This is an *Accepted Manuscript*, which has been through the Royal Society of Chemistry peer review process and has been accepted for publication.

Accepted Manuscripts are published online shortly after acceptance, before technical editing, formatting and proof reading. Using this free service, authors can make their results available to the community, in citable form, before we publish the edited article. We will replace this *Accepted Manuscript* with the edited and formatted *Advance Article* as soon as it is available.

You can find more information about *Accepted Manuscripts* in the [Information for Authors](#).

Please note that technical editing may introduce minor changes to the text and/or graphics, which may alter content. The journal's standard [Terms & Conditions](#) and the [Ethical guidelines](#) still apply. In no event shall the Royal Society of Chemistry be held responsible for any errors or omissions in this *Accepted Manuscript* or any consequences arising from the use of any information it contains.

Argon ion irradiation induced morphological instability of bare and thiol-functionalized Au(111) surfaces

Annika Venäläinen,^a Minna T. Räisänen,^b Benoît Marchand,^a Kenichiro Mizohata,^a and Jyrki Räisänen^{*a}

Received Xth XXXXXXXXXX 20XX, Accepted Xth XXXXXXXXXX 20XX

First published on the web Xth XXXXXXXXXX 200X

DOI: 10.1039/b000000x

Ar ion irradiation-induced changes in the morphology of bare and 1-dodecanethiol self-assembled monolayer (SAM) covered Au(111) surfaces have been investigated systematically. The changes were followed by scanning tunneling microscopy (STM) and X-ray photoelectron spectroscopy (XPS) measurements while varying the ion charge (Ar^+ , Ar^{4+}), energy (10 - 40 keV) and fluency (10^{12} - 10^{13} ions/cm²). The impact of flame-annealing of the Au(111) surface on subsequent ion bombardment was considered and more prominent related surface morphology changes were noted. The irradiation of Au(111) surfaces generated Au vacancy and adatom islands and caused roughening of step edges. The size and abundance of these islands and the level of deformation on the step edges depended strongly on the ion energy and fluency. In case of the SAM functionalized surface, the gold vacancy islands present on the surface already from the SAM formation were modified, step edges roughened and gold adatom islands formed. Similarly to the bare surface, the level of surface deformation increased as a function of ion energy and fluency. The Ar^{4+} irradiation caused on the average slightly larger vacancy islands on the SAM modified surfaces than the Ar^+ irradiation. Irradiation to fluency of 10^{12} ions/cm² mostly maintained standing-up orientation of the thiolates whereas irradiation to higher fluency resulted in reduced surface coverage and flat-lying molecules. As a general trend the DDT covered surfaces were more susceptible for irradiation-induced surface morphology changes than the unmodified Au surfaces.

1 Introduction

Low energy ion irradiation has been successfully used to directly synthesize nanoparticles on surfaces and in modifying already existing surface nanosystems. Typically thin film structures and nanoparticles are modified to prepare nanoparticles supported on solid surfaces. Ion etching of island thin films reduces all dimensions of the islands leading eventually to formation of nanosized particles [1]. There are several ways how the process can be controlled via the irradiation conditions. By proper choice of the nanoparticle material and ion type and energy, the sizes and locations of the patterned nanoscaled structures at surfaces can be tuned [2]. The resulting surface pattern type (e.g. clusters or nanoporous film) following thin film irradiation, can be regulated by the ion fluency [3]. The surface morphology can be controlled also by the ion incident angle or via interface kinetics [4, 5]. Also a differing approach compared to those described above has been utilized; substrate pre-treatment by ions followed by metal deposition on the irradiated surface. The density and

size of the thus formed metal clusters correlate with the surface defect density induced by the ion irradiation [6]. In general, ion irradiation is considered to provide means to process and control nanoscale supported clusters for possible electronics applications [7, 8].

Self-assembled monolayers (SAMs) are ordered molecular assemblies formed by adsorption of an active surfactant on a solid surface. They have promising applications as controlled modification of the surface with well-defined functional end groups enables new opportunities in different technological fields, such as fabrication of structured thin films, biologically active substrates and photonic materials [9, 10]. SAMs also provide convenient and archetypal means to study interactions between ions/charged particles and ordered organic systems. Such studies complement investigations of ion-induced damage in biomolecular systems as well as have relevance in development of new perspectives for ion beam lithography. The majority of studies concerning ion-SAM interactions available in the literature deal with emission processes and observation of the sputtered molecular and cluster ions [11, 12, 13]. Only one previous, very recent study concerns the morphological modifications of the SAM surfaces induced by the ion interactions [10]. In that study experiments for 1-dodecanethiol (DDT) SAMs on Au(111) were conducted using 14 keV argon ions with charge states of 7+ and 8+. The results obtained

^aDepartment of Physics, Division of Materials Physics, University of Helsinki, Finland. Fax: +358 9 191 50042; Tel: +358 9 191 50082; E-mail: jyrki.raisanen@helsinki.fi

^bDepartment of Chemistry, Laboratory of Inorganic Chemistry, University of Helsinki, Finland

by scanning tunneling microscopy (STM) and time-of-flight secondary ion mass spectrometry (TOF-SIMS) measurements lead the authors to conclude that the used irradiations induced only minor surface defects which correspond to cleavage of the uppermost hydrogen atoms from the thiolate molecules [10].

The influence of primary keV Ar ion bombardment parameters, namely charge state, energy and fluency, on the morphologies of both bare Au(111) and DDT SAM covered Au(111) surfaces are here systematically investigated by STM and X-ray photoelectron spectroscopy (XPS). DDT was chosen as it is perhaps the most widely studied molecular overlayer. Alkanethiol SAMs on gold surface in general are highly stable and readily formed due to the strong Au-S interactions and intermolecular van der Waals interactions [14]. Even though gold is the most common substrate for SAMs, the effects of ion bombardment on Au surfaces as a substrate for SAMs have not surprisingly been studied systematically earlier. The previous disconnected STM studies concern mainly structures created by highly charged $Xe^{25+,44+}$ ions and the results have not been conclusive [15, 16, 17]. The herein presented studies for Au(111) surfaces irradiated by Ar ions serve as control experiments for the irradiated DDT covered Au(111) surfaces. In this study we also consider the impact of flame-annealing of the Au(111) coated mica slide (prior the SAM growth) on subsequent ion bombardment. The current study provides a continuation for our previous works where morphologies of DDT SAM/Au(111) surfaces were investigated after gas-phase deposition of gold and other coinage metal clusters [18, 19].

2 Experimental Methods

SAM preparation. 1-Dodecanethiol (DDT, $CH_3(CH_2)_{11}SH$, purity $\geq 98\%$) was purchased from Sigma-Aldrich and used as received [20]. SAMs were prepared by immersing freshly flame-annealed Au(111) coated mica slides (300 nm Au, Georg Albert PVD) in 1 mM ethanol solution of DDT for 48 h, after which the samples were rinsed with ethanol and blow-dried with N_2 .

Ar irradiation. The argon ions were produced with a High Voltage Engineering 500 kV ion implanter. The energies used for the normally-incident Ar ions were 10, 30 and 40 keV. Typical ion current on a sample area of 5.0 cm^2 was 15 nA. All irradiations were carried out at room temperature. Since the employed irradiation fluxes were low, it is expected that insignificant amount of heat was dissipated on the samples during the irradiations. The fluency during the Ar^+ irradiations of both bare Au(111) and DDT SAM/Au(111) surfaces were 10^{12} , 5×10^{12} and 10^{13} ions/cm^2 . Bare Au(111) and DDT SAM/Au(111) surfaces were also irradiated with Ar^{4+} ions to the fluency of 10^{12} ions/cm^2 and 10^{13} ions/cm^2 .

STM Characterization. The STM measurements were conducted in constant-current mode at the Laboratory of Inorganic Chemistry under ambient conditions with a Veeco Instrument NanoScope V - MultiMode V scanning probe microscope, using a Platinum/Iridium (Pt80/Ir20) wire ($\varnothing=0.25\text{ nm}$) as tip. From the acquired STM data the deformations in the step edges and formation of Au vacancy and adatom islands on the surface were analyzed using the scanning probe microscopy data analysis software Gwyddion [21]. In calculations only isolated islands have been taken into account. Islands merged on the step edges have been overlooked. The Gwyddion programme provided the number of islands with specific size for the statistical size distributions of the vacancy and adatom islands. A typical size distribution included about 70 individual islands from which the average of the values and standard deviations were calculated. The standard deviation of the average values was estimated to be 10% taking into account the pixel resolution of the STM images when determining the island areas. The elapsed time between the irradiations and the STM measurements was kept similar for all samples ($\sim 24\text{ h}$). The time regime was determined by the fact that in case of irradiated Au(111) surfaces after 500 min no mass transfer takes place and the defect island size does not change [22]. The stability of the studied surface structures at room temperature was investigated by repeated imaging with STM (intervals of several days), showing unaltered morphology both for irradiated Au(111) surfaces and for irradiated DDT covered surfaces.

XPS Characterization. XPS data was obtained using an Hiden Analytical SIMS/SNMS/XPS system, equipped with an Mg K_{α} X-ray source (Omicron DAR 400) operated at 75 W and a 5° electron take-off angle. The photoelectrons were analyzed by an Argus spectrometer (detector angle 65°) with 50 eV pass energy. In order to minimize charging effect and to minimize film deterioration, electron suppression (intensity = 300 nA, $E=1\text{ eV}$) was used. The plane to detector angle was $\theta = 60^\circ$.

3 Results and Discussion

3.1 Ar-ion irradiated Au(111) surfaces

3.1.1 The effect of substrate flame-annealing. In the preparation of SAMs, the Au substrates are typically flame-annealed resulting in a reconstructed surface and removal of any possible surface contaminants. Annealing also increases surface area of the atomically flat terraces even by a factor of 25 relative to a non-annealed surface [23]. Herein the effect of the sample preparation protocol was studied with respect to ion irradiation-induced surface morphological changes. One Au(111) substrate was flame-annealed and the other one was used in an as-received condition (the gold substrates had been

stored in a vacuum after receiving them from the manufacturer) prior 40 keV Ar^+ irradiation to the fluency of 10^{13} ions/cm².

STM characterization and subsequent data analysis of these samples clearly show irradiation-induced changes on their surface morphologies (Table 1, Figures 1 and 2). The flame-annealed and non-annealed surfaces prior the irradiation are characteristic Au(111) surfaces with large terraces and monoatomic high (ca. 2.4 Å) step edges. Irradiation roughens strongly the step edges of both surfaces. This is logical as the gold atoms are most mobile at those positions [24]. After the irradiation also two types of newly formed nanoislands are visible on the surfaces. The protrusions appear in the STM images as bright spots whereas the pits can be visualized as dark holes. Heights (2.4–9.6 Å) and depths (2.4–7.2 Å, i.e. multiples of 2.4 Å) of the protrusions and the pits match the dimension(s) of Au atom(s) suggesting that the former consist of gold adatoms and the latter are gold vacancy islands. The formation of such pits and one atomic layer high adatom islands has been noted previously after 500 eV Ar-ion sputtering at room temperature [25]. The morphological studies reveal that both types of nanoislands (i.e. adatoms and vacancies) are observed throughout the surfaces, including the middle parts of the gold terraces, and that quite often the gold adatoms locate at the edges of the vacancy islands. Both on the annealed and on the non-annealed surfaces the adatom islands have on average a much larger surface area than the vacancy islands (Table 1).

Table 1 Statistical analysis of the Au vacancy/adatom islands formed on the flame-annealed and non-annealed Au(111) surfaces by 40 keV Ar^+ ion irradiation to the fluency of 10^{13} ions/cm²

	Vacancy island	Adatom island
Average projected surface area (nm²)		
flame-annealed substrate	25.9±2.6	66±7
non-annealed substrate	25.3±2.5	51±5
Depth/Height (nm)		
flame-annealed substrate	0.24-0.72	0.24-0.96
non-annealed substrate	0.24-0.48	0.24-0.72
Abundance (μm⁻²)		
flame-annealed substrate	895	655
non-annealed substrate	530	770
Total surface area (%)		
flame-annealed substrate	2	4
non-annealed substrate	1	4

The irradiation-induced Au adatom islands are higher on the flame-annealed surface than on the non-annealed surface. Irradiation affects also the abundances and surface areas of the formed nanoislands (Table 1, Figures 1 and 2). The gold va-

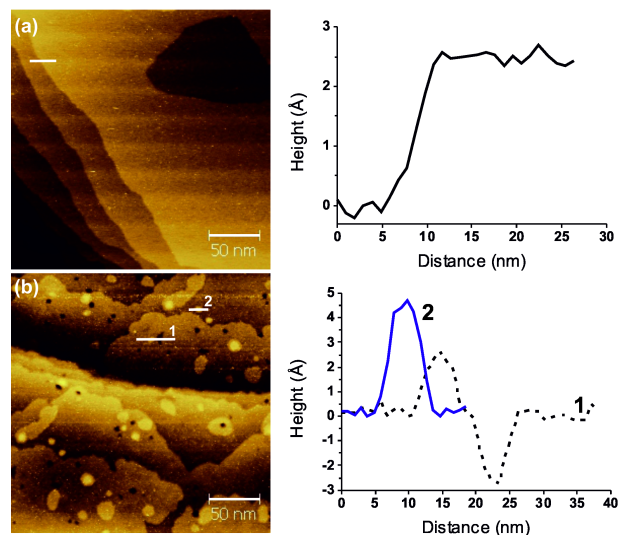


Fig. 1 Large-scale STM images of a flame-annealed Au(111) surface (a) prior and (b) after 40 keV Ar^+ irradiation to the fluency 10^{13} ions/cm². Height profiles along the lines shown in the images are presented on the right. Imaging conditions $V_b = 150 - 300$ mV, $I_t = 80$ pA

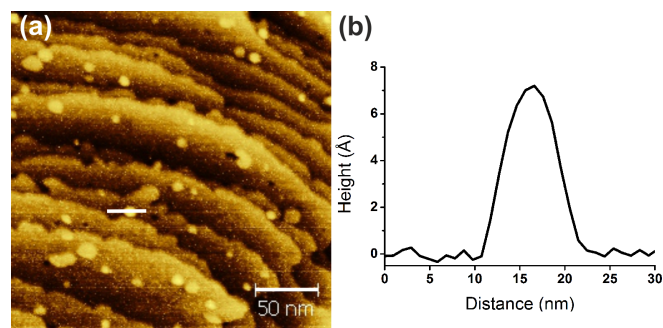


Fig. 2 (a) A large-scale STM image of a non-annealed Au(111) surface irradiated with 40 keV Ar^+ ions to the fluency 10^{13} ions/cm². (b) Height profile along the line shown in image a. Imaging conditions $V_b = 300$ mV, $I_t = 80$ pA. STM image of the surface prior the irradiation appears similar to that of the flame-annealed surface presented in image a

cancy islands are significantly more abundant ($895 \mu\text{m}^{-2}$ vs. $530 \mu\text{m}^{-2}$) and deeper (see Table 1) on the annealed surface than on the non-annealed surface. The difference in surface areas is most obvious for the gold adatom islands which on average are clearly larger on the annealed surface (66 nm^2 vs. 51 nm^2). It is proposed that the adatom islands created on the annealed surfaces have merged together to form larger islands via adatom-mediated Ostwald ripening mechanism. A possible source of adatoms is also the lifting of the herringbone reconstruction due to the Ar-ion irradiation providing

reactive Au adatoms [26]. On the whole the STM data suggest that annealing of the substrate makes it more susceptible to irradiation-induced surface defects but no specific single cause for this can be pointed out. The topography of the annealed Au(111) surface is characterized by large, atomically flat terraces separated mostly by monoatomic steps of 2.4 Å in height. As the atoms located on elevated parts of the Au(111) surface have lower binding energy, they can thus be more easily moved without introducing defects in other parts of the surface. Also the long-range elastic strain introduced in the reconstructed layer could play a role. Furthermore, it has been reported that the Au(111) reconstruction affects the local reactivity of the surface and the Au atoms in the transition regions are the most reactive, in line with the present finding [24]. All subsequent experiments in this study were carried out by utilizing the flame-annealed substrates which are used more conventionally.

3.1.2 The effect of Ar ion energy. For HOPG, mica, CaF_2 and Si surfaces the size of the ion irradiation generated structures has been noted by scanning probe microscopy to be nearly independent of the highly charged ion kinetic energy [17]. In case of Au surfaces, the effects of bombarding ion energy have been studied only in terms of sputtering yield but not from the surface morphology point of view. Here we study the effect of irradiation energy by STM with a set of experiments using 10, 30 and 40 keV Ar^+ ions to a fluency of 10^{12} ions/cm². While 10 keV ions do not seem to cause any surface deformation, pits (2.4–7.2 Å in depth) interpreted as gold vacancy islands have been formed on the surfaces irradiated with 30 and 40 keV ions (Figure 3). It also seems that the vacancy islands are more abundant on the surface irradiated with 40 keV ions (abundance $125 \mu\text{m}^{-2}$) than on the surface treated with 30 keV ions (abundance $65 \mu\text{m}^{-2}$). On the other hand, no definitive vacancy/adatom island area dependency as a function of ion energy was noted.

3.1.3 The effect of fluency. Also the effect of bombarding ion fluency on Au surface has been studied in the literature only in terms of sputtering yield. For 30 keV Ar^+ projectiles the sputtering yield for Au at low fluencies ($< 10^{14}$ ions/cm²) has been found to be nearly independent on fluency but at higher fluencies the sputtering yield becomes fluency dependent due to trapped projectiles which change the sample composition [27].

Here two different sets of experiments were carried out to study the effect of fluency on the deformation of Au(111) surface. In the first set, 30 keV Ar^+ irradiation was used to the fluencies of 10^{12} , 5×10^{12} and 10^{13} ions/cm². While irradiation to the lowest fluency produces only a small number of gold vacancy islands on the surface (Figure 3b), irradiations to the higher fluencies affect the Au(111) surface also in other ways (Figure 4). Step edges on these surfaces are clearly de-

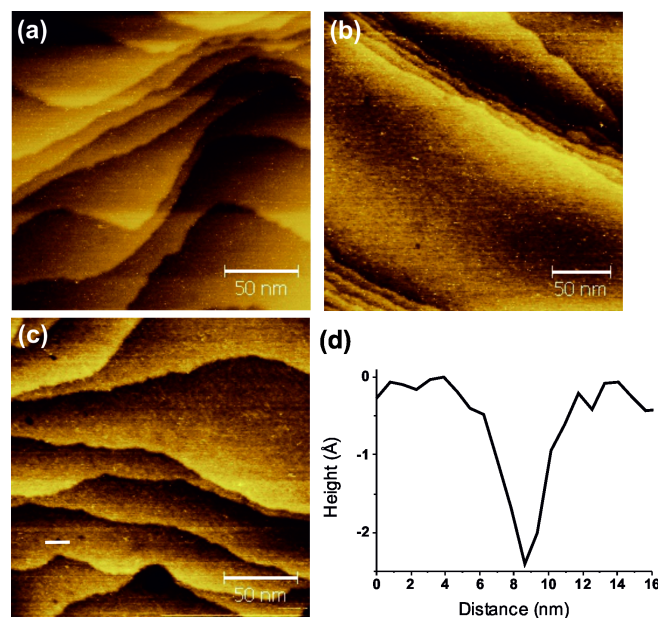


Fig. 3 STM images of Au(111) surfaces irradiated with (a) 10 keV, (b) 30 keV and (c) 40 keV Ar^+ ions to the fluency of 10^{12} ions/cm². Imaging conditions $V_b = 150$ mV, $I_t = 80$ pA. (d) Height profile along the line shown in image c. The number of Au vacancy islands is $65 \mu\text{m}^{-2}$ after 30 keV irradiation and $125 \mu\text{m}^{-2}$ after 40 keV irradiation. Average surface area of the vacancy islands is 18.0 ± 1.8 nm² after 30 keV irradiation and 18.1 ± 1.8 nm² after 40 keV irradiation

formed being rougher than on the surface irradiated to the lowest fluency or on the non-irradiated surface and gold adatom islands are formed throughout the surfaces. On the surface irradiated to the fluency of 10^{13} ions/cm² also new type of protruding islands, not observed on the other surfaces, are clearly visible and abundant (Figure 4b). These islands appear in the STM images in a slightly darker shade than the gold adatom islands their height (1.5 Å, Figure 4c) matching well with the dimension of argon atoms [28]. It should be noted that similar structures were observed also for samples irradiated with 25 keV Ar ions to the fluency of 10^{13} ions/cm². The projected range of the implanted 30 keV Ar ions in amorphous Au is ~ 11 nm [29] indicating that (also in case of the irradiated Au(111) surface) the Ar atoms can be expected to locate deeper in the bulk. Indeed, XPS analysis showed neither Ar atoms nor additional elements (see XPS section). The sampling depth for XPS under these conditions is approximately 4 nm, i.e., well below the implantation depth of the Ar ions, suggesting that the Ar atoms lie deeper in the Au(111) substrate [30]. Protrusions with similar height have been noted also in a recent study [22] where Au(111) surfaces were irradiated by 2 keV Ar ions to the fluency of 7×10^{15} ions/cm². The authors proposed that such protrusions are caused by trapped Ar

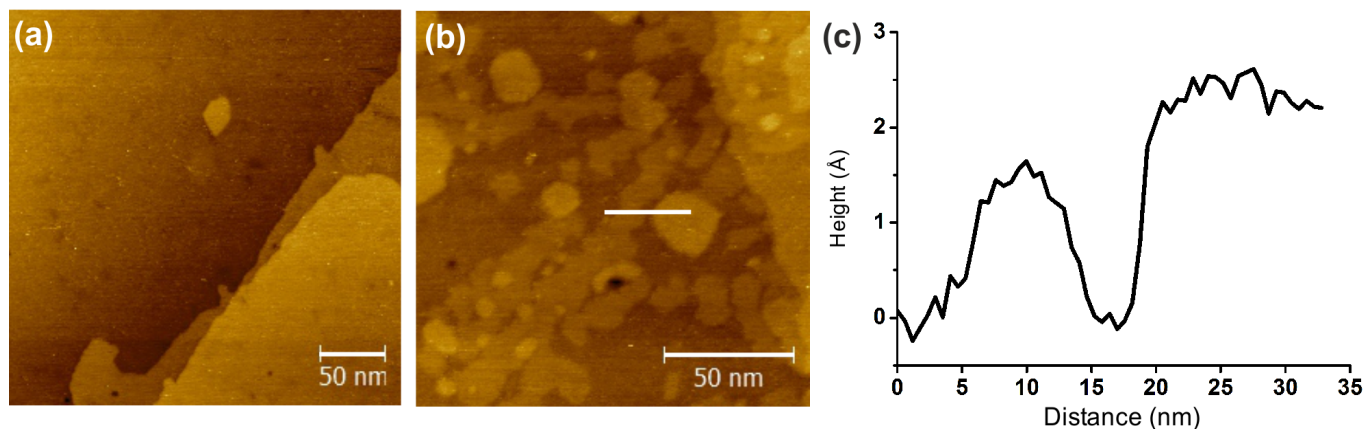


Fig. 4 STM images of Au(111) surfaces irradiated with 30 keV Ar^+ ions to the fluency of (a) 5×10^{12} ions/cm² and (b) 10^{13} ions/cm². (c) Height profile along the line shown in image b. Imaging conditions $V_b = 150 - 200$ mV, $I_t = 80 - 150$ pA

atoms as bubbles in the sub-surface region. The origin of the currently noted islands will be studied in the future in more detail also by investigating the effect of energy and fluency dependency.

Statistical analysis of the STM data (Table 2) reveals that, as expected, the highest fluency causes most significant changes on the morphology of Au(111) surface and thus there is a clear dependence between the fluency and the level of surface deformation. The results show stepwise progression of the surface deformation. First gold vacancy islands are formed, then gold adatom islands and finally the trapped sub-surface Ar atoms induce visible surface deformations (at the fluency of 10^{13} ions/cm²), referred to as Ar islands in Table 2. The higher adatom islands noted at the higher fluencies could be a result of overlapping events at locations close to each other forming thus extended defects.

The second set of experiments was conducted with 40 keV Ar^+ irradiation to the fluencies of 10^{12} and 10^{13} ions/cm². The higher fluency causes roughening of the step edges and formation of numerous gold vacancy and adatom islands (depths 2.4-7.2 Å, heights 2.4-9.6 Å, see Figure 1b and Table 1) while with the lower fluency the formation of gold vacancy islands (depths 2.4-7.2 Å) is significantly less frequent (Figure 3c). Thus also in case of 40 keV Ar^+ ions it can be concluded that the higher the ion irradiation fluency is, the higher is the level of Au(111) surface deformation.

3.2 Ar ion irradiation of DDT SAM covered Au(111) surface

Quality of the DDT SAMs was confirmed by STM both prior and after the irradiations from the sample surface unexposed to the irradiation. STM images of the non-irradiated surfaces (Figure 5) show characteristic thiolate SAM covered

Table 2 The effect of 30keV Ar^+ ion fluency on the Au(111) surface indicating the characteristics of the formed gold vacancy and adatom islands.

	Vacancy island	Adatom island	Ar island
Average projected surface area (nm²)			
10^{12} ions/cm ²	18.0±1.8	-	-
5×10^{12} ions/cm ²	35.1±3.5	86±9	-
10^{13} ions/cm ²	15.5±1.6	20.8±2.1	75±8
Depth/Height (nm)			
10^{12} ions/cm ²	0.24-0.72	-	-
5×10^{12} ions/cm ²	0.24-0.72	0.24	-
10^{13} ions/cm ²	0.24-0.72	0.24-0.48	0.15
Abundance (μm⁻²)			
10^{12} ions/cm ²	65	-	-
5×10^{12} ions/cm ²	55	20	-
10^{13} ions/cm ²	135	1380	1070
Total surface area (%)			
10^{12} ions/cm ²	0.1	-	-
5×10^{12} ions/cm ²	0.2	0.2	-
10^{13} ions/cm ²	0.2	2.8	8.0

Au surfaces with monoatomic deep (2.4 Å) gold vacancy islands (formed during the SAM formation process) and densely packed thiolate molecules in a hexagonal arrangement and in an upright orientation [31].

3.2.1 The effect of bombarding ion charge state. The effect of Ar ion charge state was studied with a 40 keV irradiation to a fluency of 10^{13} ions/cm² and using charge states of 1+ and 4+. The impact of Ar^{q+} ($4 \leq q \leq 10$) ion bombardment

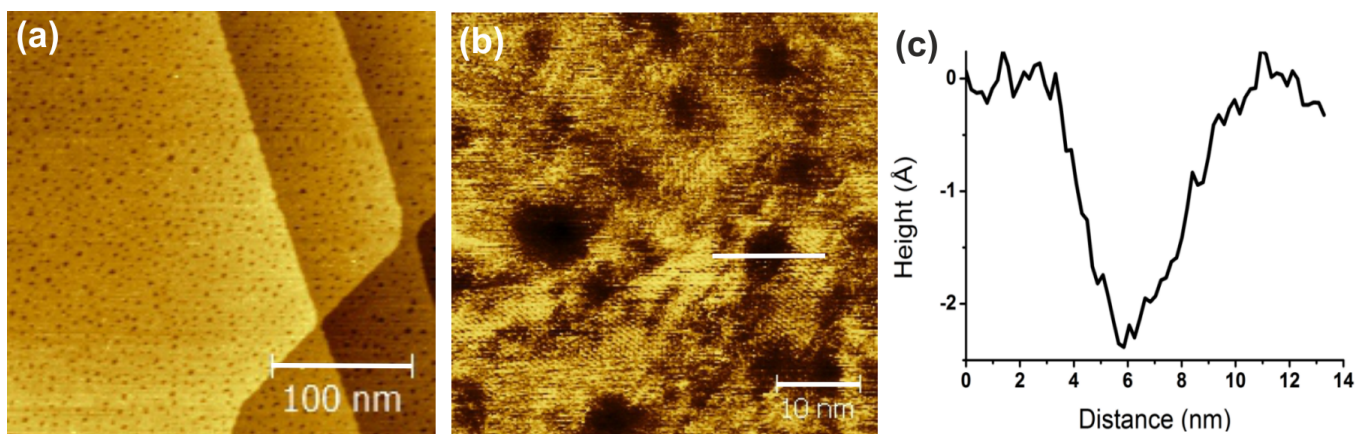


Fig. 5 (a) A large-scale and (b) a high-resolution STM image of the non-irradiated DDT SAM/Au(111) surface. (c) Height profile along the line shown in image b. Imaging conditions $V_b = 650 - 900$ mV, $I_t = 20 - 30$ pA

with kinetic energies from 2 to 18 keV on DDT SAM covered gold surfaces has been studied by Flores et al. by following the emitted proton yields [32]. They concluded that the proton yields increase with increasing charge state q , scaling as q^γ , with $\gamma \sim 5$. Thereby it can be anticipated that the charge state of $4+$ has a more significant effect on the surface morphology than that of $1+$. STM imaging reveals that in addition to significant deformation of the step edges, Au adatom and vacancy islands are respectively formed and being modified on the DDT SAM covered Au surfaces upon irradiation with both charge states (Figures 6 and 7). As the vacancy islands are formed on the surfaces already during the SAM formation process (see Figure 5), it is difficult to discern them from the possible irradiation-induced depressions. However, statistical analysis of the STM images (Table 3) shows that in comparison to the non-irradiated surface, the vacancy islands are on both irradiated surfaces on the average larger in size and significantly less abundant. Interestingly, the total combined surface area of the Au vacancy islands and the adatom islands on both irradiated surfaces is close to the total surface area of the vacancy islands on the non-irradiated surface.

Gold vacancy islands are on the average slightly larger on the Ar^{4+} irradiation modified DDT SAM surfaces than on the Ar^+ modified surfaces. This finding is in agreement with the observations of Flores et al. and could be related to charge neutralization [32]. The depth of the vacancy islands and height of the adatom islands on the other hand seem not to be affected by the ion charge state. The vacancy island depth is the same as noted for the non-irradiated DDT SAM/Au(111) surface (see Table 3). It should be noted that in the irradiation of the bare Au(111) surface the ion charge state did not have any noticeable effect. This is as expected since in case of highly charged ion irradiations it has been noted that the volume of the vacancy and adatom islands increases as a

Table 3 Effect of ion charge state to the formation of Au vacancy/adatom islands on DDT SAM/Au(111) surfaces irradiated with 40 keV Ar^+ and Ar^{4+} ions to the fluency of 10^{13} ions/cm²

	Vacancy island	Adatom island
Average projected surface area (nm²)		
non-irradiated	16.7±1.7	-
Ar^+	23.7±2.4	40±4
Ar^{4+}	25.8±2.6	32.1±3.2
Depth/Height (nm)		
non-irradiated	0.24	-
Ar^+	0.24-0.48	0.24-1.20
Ar^{4+}	0.24-0.48	0.24-1.20
Abundance (μm⁻²)		
non-irradiated	5555	-
Ar^+	775	900
Ar^{4+}	1750	1400
Total surface area (%)		
non-irradiated	9	-
Ar^+	2	4
Ar^{4+}	5	5

function of the charge state only after certain case-specific, threshold charge state (q_{th}). This effect has been observed for highly oriented pyrolytic graphite (HOPG, $q_{th} \sim 17$), mica ($q_{th} \sim 30$), CaF_2 ($q_{th} \sim 18$) and Si ($q_{th} \sim 30$) surfaces [17]. On a molecular-level, both irradiated DDT SAM/Au(111) surfaces appear to be similar as areas with flat-lying molecules (visualized as striped-phases with inter-row distances of 1.5 nm) are visible and closely-packed molecules in a hexagonal arrangement are not observed anymore (Figures 6b and 7b). In the flat-lying orientation alkyl chains of the molecules form

an interdigitated bilayer (inter-row periodicity of 1.5 nm) on the Au surface [33]. It is very likely that thiolate coverages are reduced on the surfaces due to the irradiation irrespective of ion charge state.

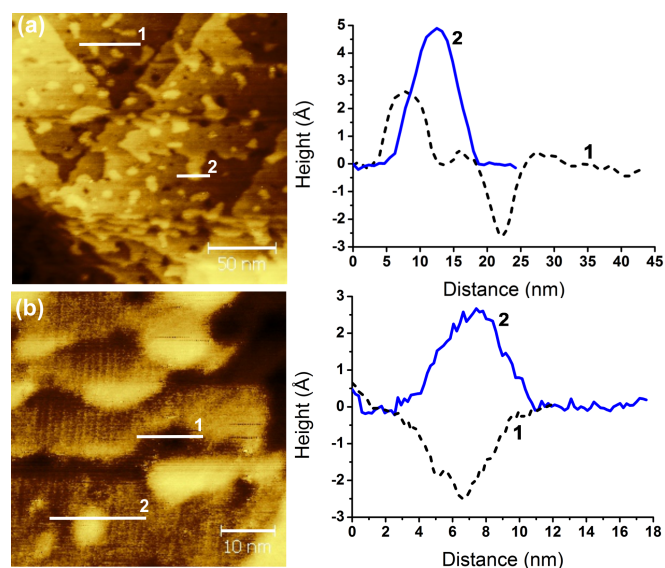


Fig. 6 (a) Large-scale and (b) high resolution STM images of DDT SAM/Au(111) surfaces irradiated with 40 keV Ar^+ ions to the fluency of 10^{13} ions/ cm^2 . Height profiles along the lines shown in images a and b are presented on the right. Imaging conditions $V_b = 400 - 600$ mV, $I_t = 30$ pA

3.2.2 The effect of Ar ion energy. The effect of Ar^+ ion energy on the DDT SAM/Au(111) surface was studied using 10 and 40 keV irradiations to a fluency of 10^{12} ions/ cm^2 . In case of the SAM modified surface, even the 10 keV irradiation induces formation of gold adatom islands and deformation of the step edges (Figure 8). The energy loss of the Ar ions in the DDT layer can be estimated by calculations [29]. For 10 keV Ar ions the energy loss is ~ 75 eV and for 40 keV ions about 88 eV, assuming a layer thickness of 1.4 nm [34]. Therefore the noted effect for 10 keV ions is not unexpected as both 10 keV and 40 keV Ar ions lose minor amount of energy within the SAM layer. In addition, the gold vacancy islands are significantly less abundant than on the non-irradiated DDT SAM/Au(111) surface as their number has reduced approximately by half ($2220 \mu m^{-2}$ vs. $5555 \mu m^{-2}$, Table 4). Since the vacancy/adatom islands are deeper/higher in case of the 40 keV irradiation and taking into account other changes on the surfaces it can be concluded that the level of surface deformation on the DDT SAM modified Au(111) surface increases with the ion energy (see Table 4 and Figures 8 and 9). The number of gold adatom islands and total coverages of gold adatom and vacancy islands are significantly higher on the surface treated with 40 keV ions than on the surface

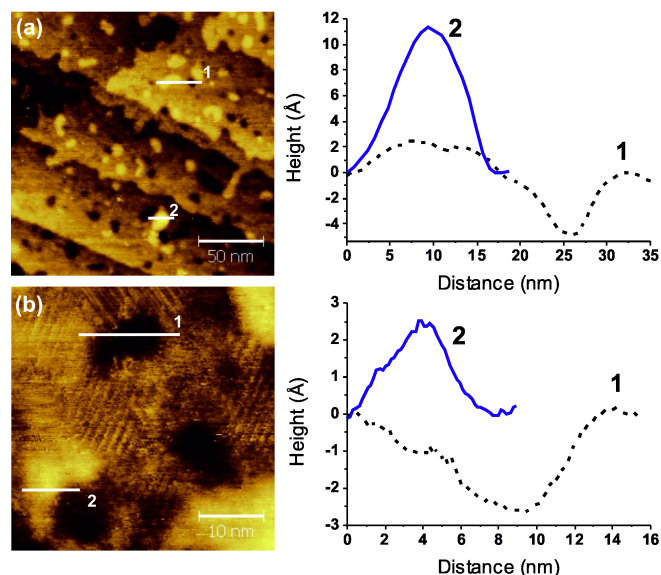


Fig. 7 (a) A large-scale STM image and (b) a molecularly resolved image of DDT SAM/Au(111) surfaces irradiated with 40 keV Ar^{4+} ions to the fluency of 10^{13} ions/ cm^2 . Height profiles along the lines shown in images a and b are presented on the right. Imaging conditions $V_b = 900$ mV, $I_t = 20$ pA

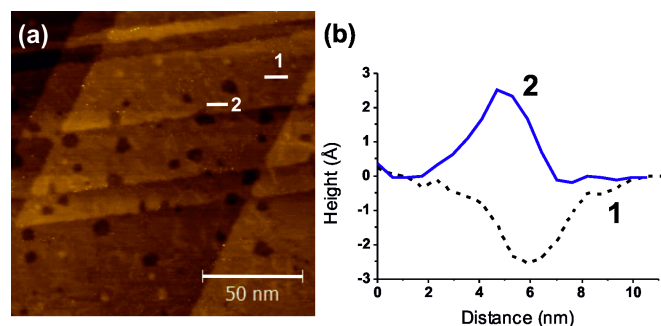


Fig. 8 (a) Large-scale STM image of the DDT SAM/Au(111) surface irradiated with 10 keV Ar^+ ions to the fluency of 10^{12} ions/ cm^2 . (b) Height profiles along the lines shown in image a. Imaging conditions $V_b = 500$ mV, $I_t = 30$ pA

treated with 10 keV ions. The irradiation with the higher energy ions also results in more deformed step edges. In the corresponding irradiations of the bare Au(111) substrates no clear energy dependency was noted. Taking this into account and the fact that the ions lose insignificant amount of energy within the DDT layer, it can be concluded that the noted surface morphology changes are strongly related to the presence of the DDT layer.

High-resolution STM images of surfaces irradiated with 10 and 40 keV ions show thiolate molecules on the surface in a closely-packed arrangement with a standing-up orientation but

Table 4 Effect of 10 and 40 keV Ar^+ irradiation energy (fluency 10^{12} ions/cm²) on formation of Au vacancy/adatom islands on the DDT SAM/Au(111) surface

	Vacancy island	Adatom island
Average projected surface area (nm²)		
non-irradiated	16.7±1.7	-
10 keV	15.2±1.5	12.9±1.3
40 keV	22.3±2.2	32.1±3.2
Depth/Height (nm)		
non-irradiated	0.24	-
10 keV	0.24-0.48	0.24
40 keV	0.24-1.20	0.24-0.72
Abundance (μm⁻²)		
non-irradiated	5555	-
10 keV	2220	620
40 keV	2095	1375
Total surface area (%)		
non-irradiated	9	-
10 keV	3	1
40 keV	5	4

also small areas where the molecules have adopted a flat-lying orientation (Figure 9b). The observed inter-row periodicity of 1.5 nm (height profile 3 in Figures 9b and c) and 0.5 nm periodicity along the stripe (height profile 4 in Figures 9b and c) in these areas are consistent with flat-lying DDT molecules whose alkyl chains form an interdigitated bilayer on the Au surface [34]. The change in orientation indicates that the irradiation interferes with the Au-SAM interactions as well as the van der Waals interactions between the thiol chains, resulting in a reduced surface coverage of thiols [35].

3.2.3 The effect of fluency. By keeping the irradiation fluency reasonably low, the surface damage due to single ion impact can be resolved by STM [10]. STM imaging and following statistical analysis (Table 5) of DDT SAM/Au(111) surfaces irradiated with 40 keV Ar^+ ions to fluencies of 10^{12} ions/cm² (Figure 9) and 10^{13} ions/cm² (Figure 6) reveal that the irradiation fluency affects the level of surface deformation in an expected way. The surface irradiated to the higher fluency is significantly more deformed on step edges and has larger gold adatom and vacancy islands than the other surface. The abundance of the isolated nanoislands is higher on the surface irradiated to the lower fluency but it is probable that on the other surface the defect formation is already so frequent that the formed defects have merged together and migrated to the step edges. The adatom islands are higher in case of the higher fluency indicating presence of overlapping events as in case of bare Au(111) surface. Thiolate molecules on the sur-

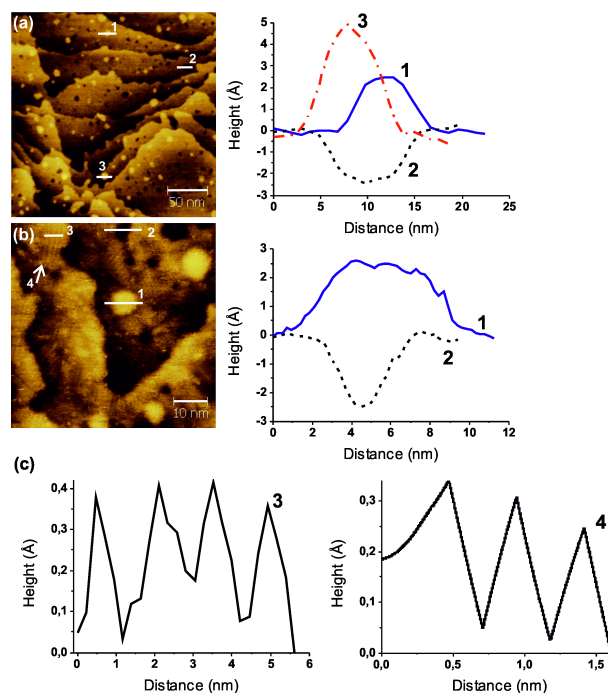


Fig. 9 (a) Large-scale STM image, and (b) molecularly resolved image of the DDT/Au(111) surface irradiated with 40 keV Ar^+ ions to the fluency of 10^{12} ions/cm². Height profiles of Au adatom and vacancy islands along the lines shown in images a and b are presented on the right. Imaging conditions $V_b = 650$ mV, $I_t = 30$ pA. (c) Height profiles showing inter-row periodicity (line 3 in image b) and periodicity along the stripe (indicated by an arrow 4 in image b) in the region with flat-lying molecules. The high-resolution images of the surface irradiated with 10 keV Ar^+ ions (fluency of 10^{12} ions/cm²) show similar changes in the SAM as seen in Fig. 9b

face irradiated to the fluency of 10^{12} ions/cm² are still mostly closely-packed and in a standing-up orientation (Figure 9b) whereas the irradiation to the fluency of 10^{13} ions/cm² results in a reduced thiolate coverage and flat-lying molecules (Figure 6b).

As noted earlier all ions studied in this work lose approximately same, insignificant, amount of energy within the DDT layer. It can be noted that a general clear trend is that the irradiated DDT surfaces show more significant change in the morphology than the irradiated bare Au(111) surfaces. This can be explained by Ar ion stimulated vacancy mediated Ostwald ripening enhanced by the presence of the DDT monolayer which increases the excess of adatoms and vacancies and thus the mobility at the Au(111) surface [36].

3.2.4 Ar ion irradiation-induced chemical and molecular level effects studied by XPS. XPS was used to ascertain the irradiation-induced chemical and molecular-level effects on the DDT SAM modified Au(111) surfaces. For this pur-

Table 5 The effect of fluency on the formation of Au vacancy/adatom islands on the DDT SAM/Au(111) surfaces irradiated by 40 keV Ar^+ ions

	Vacancy island	Adatom island
Average projected surface area (nm^2)		
non-irradiated	16.7±1.7	-
10^{12} ions/ cm^2	22.3±2.2	32.1±3.2
10^{13} ions/ cm^2	23.7±2.4	40±4
Depth/Height (nm)		
non-irradiated	0.24	-
10^{12} ions/ cm^2	0.24-0.48	0.24-0.72
10^{13} ions/ cm^2	0.24-0.48	0.24-1.20
Abundance (μm^{-2})		
non-irradiated	5555	-
10^{12} ions/ cm^2	2095	1375
10^{13} ions/ cm^2	775	900
Total surface area (%)		
non-irradiated	9	-
10^{12} ions/ cm^2	5	4
10^{13} ions/ cm^2	2	4

pose, a surface showing high level of deformation and vast number of formed nanoislands in the STM imaging (Figure 10), namely the surface irradiated with 30 keV Ar^+ ions to the fluency of 10^{13} ions/ cm^2 , was chosen for the XPS studies (Table 6 and Figure 11). Non-irradiated DDT SAM/Au(111) surface was used as a reference sample also in the XPS studies.

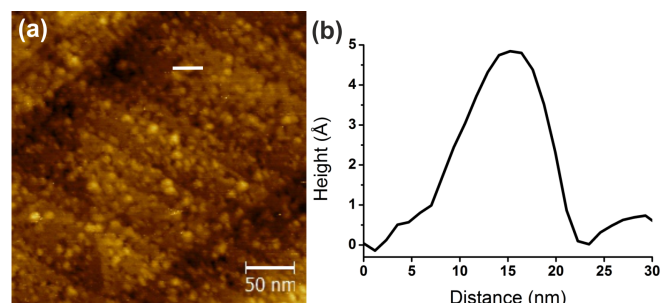


Fig. 10 A large-scale STM image of DDT SAM/Au(111) surface irradiated with 30 keV Ar^+ ions to the fluency of 10^{13} ions/ cm^2 . Due to the high level of deformation, statistical analysis of the data concerning the areas of the islands was not feasible. (b) Height profile along the line shown in image a. Imaging conditions $V_b = 500$ mV, $I_t = 50$ pA

In case of the reference SAM, the S $2p_{3/2}$ signal at the BE of ca. 161 eV is assigned to bound thiolate sulphur with a different binding chemistry and/or geometry as compared to

Table 6 S $2p_{3/2}$, C 1s and O 1s core levels of the DDT SAM/Au(111) surface prior and after 30 keV Ar^+ irradiation to the fluency of 10^{13} ions/ cm^2

	S $2p_{3/2}$		C 1s		O 1s
	BE (eV)	Amount (%)	BE (eV)	Amount (%)	BE (eV)
prior irradiation	160.7	7	284.7	91	533.0
DDT SAM/Au	161.8	72	286.2	6	
	163.0	21	287.7	4	
after irradiation	160.7	15	284.4	91	532.7
DDT SAM/Au	161.8	62	286.3	6	
	163.0	23	287.7	3	

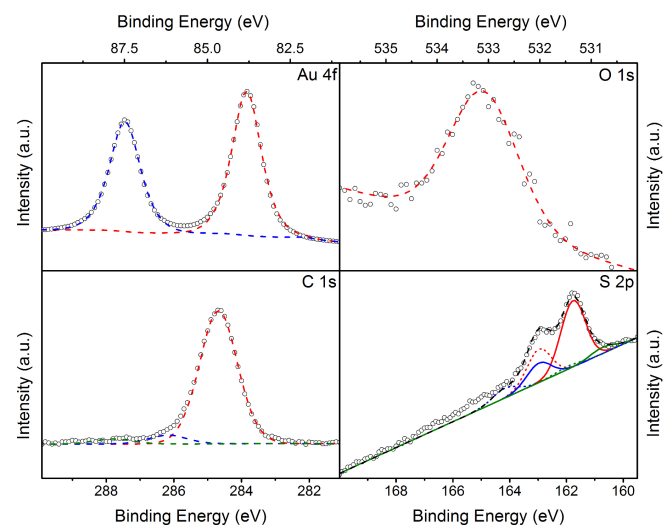


Fig. 11 XPS spectra of the Au $4f_{7/2}$, O 1s, C 1s and S $2p_{3/2}$ core levels of the DDT SAM/Au(111) surface after 30 keV Ar^+ irradiation to the fluency of 10^{13} ions/ cm^2 . The open symbols correspond to the experimental data

the typical thiolate species on Au [37, 38, 39, 40]. In case of the irradiated DDT SAM, the corresponding signal (with relative intensity of ~15% which is twice as high as that observed for the reference SAM) is proposed to arise both from the thiolate-type sulphur atoms bound to the Au surface and from elemental sulphur [41]. Both experimental SIMS studies and molecular dynamics (MD) simulations of alkanethiol SAMs on gold surface bombarded with Ar ions have also revealed formation of atomic sulfur species [42].

The S $2p_{3/2}$ signal at the BE of ca. 163 eV has almost the same relative intensity both in the reference SAM (~21%) and in the irradiated SAM (~23%) and it is assigned to irradiation-induced sulphur species formed during the XPS measurement [43, 44]. No oxidized sulphur species (BE>166 eV) [44] are

observed in the spectra of the reference and irradiated SAMs even though small amounts of oxygen could be detected on both surfaces. Similar observations have been reported previously in the literature [43].

The C 1s region in the XPS spectra of the non-irradiated and irradiated DDT SAMs exhibit a main emission near 284 eV (intensity 91% of the total amount of carbon) and small shoulders at BEs of ca. 286 eV (intensity 6%) and 288 eV (intensity \sim 3%). The main C 1s signal is related to the hydrocarbon chain of the adsorbed thiolates whereas the other signals can be assigned to carbons bound to oxygen [38, 43]. The main C 1s emission peak shifts from 284.7 to 284.4 eV upon the Ar^+ irradiation which clearly suggests that the thiolates have adopted a flat-lying orientation on the irradiated surface [41]. Moreover, the fitted peak width (full width at half-maximum, fwhm) of the emission line is 1.32 eV for the reference DDT SAM, whereas for the irradiated DDT SAM it is 1.46 eV. This indicates that the irradiated SAM is structurally less homogeneous than the reference SAM. High-resolution STM images (Figures 6b, 7b and 9b) of the irradiated DDT SAM covered surfaces confirm these results. XPS studies also suggest that irradiation with 30 keV Ar^+ ions to the fluency of 10^{13} ions/cm² breaks S-C bonds in the SAM. They are more prone to break than C-C bonds as their respective bond energies are 2.6 eV and ca. 4 eV [42]. It is evident that the weaker Au-S bonds break (bond energy 1.7 eV) also, but subsequent re-adsorption of the thiolate molecules takes place [45]. The relative intensity of the Au signal was observed to increase upon the Ar^+ irradiation while the intensity of the C signal decreased indicating diminished carbon content. The ratios of Au 4f_{7/2} : C 1s : S 2p_{3/2} signals are ca. 10:12:1 and 12:11:1 for the non-irradiated and irradiated surfaces, respectively. The C:S ratio of the reference SAM is as expected.

4 Conclusions

The present findings indicate prominent surface morphology changes on Ar ion irradiated bare and 1-dodecanethiol (DDT) covered Au(111) surfaces and show dominant substrate effects which have not been considered earlier. As a general trend the DDT covered surfaces were more susceptible for irradiation induced surface morphology changes than the unmodified Au surfaces. The irradiation was observed in general to generate Au vacancy and adatom islands and cause roughening of step edges on the bare Au(111) surface. The size and abundance of these islands as well as the level of deformation on the step edges depends strongly on the ion energy and fluency. The correlations between ion energy and fluency, and the average projected surface area of vacancy and adatom islands of the irradiated Au(111) surfaces are collected to Figure 12a.

The irradiation of DDT SAM functionalized Au(111) surfaces roughens the step edges, generates gold adatom islands

and decreases the number of vacancy islands (the latter are generated on the surface already during the SAM formation process). The surface modification occurs in such a way that the combined defect island surface areas are roughly the same before and after the irradiation. Surface deformation increases as a function of ion energy and fluency and the gold vacancy islands are on the average slightly larger on the Ar^{4+} irradiation modified surfaces than on the Ar^+ modified surfaces. Closer inspection reveals that the thiolate molecules remain mostly closely-packed and in a standing-up orientation on the surface irradiated to the fluency of 10^{12} ions/cm² whereas irradiation to the fluency of 10^{13} ions/cm² results in their reduced surface coverage and flat-lying molecules. The correlations between ion energy, fluency and charge state, and the average projected surface area of vacancy and adatom islands of the irradiated DDT SAM covered Au(111) surface are collected to Figure 12b. In a previous study only minor surface defects, corresponding to cleavage of the uppermost hydrogen atoms from the thiolate molecules, were observed when DDT SAM functionalized Au(111) surface was irradiated with 14 keV Ar ions (to the unreported fluency) [10].

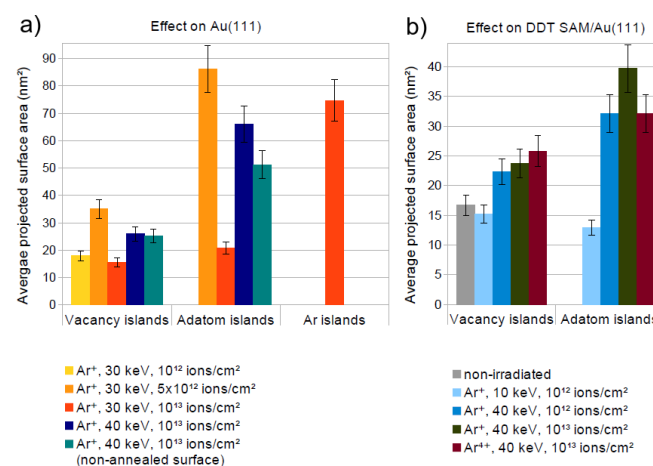


Fig. 12 a) The correlations between ion energy and fluency, and the average projected surface area of vacancy and adatom islands of the irradiated Au(111) surfaces. b) The correlations between ion energy, fluency and charge state, and the average projected surface area of vacancy and adatom islands of the irradiated DDT SAM covered Au(111) surface. Note that no adatom islands were present in the non-irradiated sample.

Acknowledgement

The doctoral program in Materials Research and Nanosciences (MATRENA) of Helsinki University is acknowledged. Support from the Academy of Finland

through projects 251531 and 263439 is acknowledged.

References

- Z. Pászti, G. Pető, Z. Horváth, O. Geszti, A. Karacs, and L. Guzzi, "Nanoparticle formation induced by low-energy ion bombardment of island thin films," *Applied Physics A: Materials Science & Processing*, vol. 76, pp. 577–587, 2003.
- B. Satpati and B. N. Dev, "Replicating Nanostructures on Silicon by Low Energy Ion Beams," *Nanotechnology*, vol. 16, no. 4, p. 12, 2004. [Online]. Available: <http://arxiv.org/abs/cond-mat/0410422>
- D. Q. Yang, E. Sacher, and M. Meunier, "The creation of Au nanoscale surface patterns by the low energy Ar⁺ beam irradiation of Au clusters evaporated onto a SiO₂/Si surface," *Applied Physics A: Materials Science and Processing*, vol. 80, pp. 575–579, 2005.
- N. Toyoda, T. Mashita, and I. Yamada, "Nano structure formation by gas cluster ion beam irradiations at oblique incidence," in *Nuclear Instruments and Methods in Physics Research, Section B: Beam Interactions with Materials and Atoms*, vol. 232, 2005, pp. 212–216.
- K. H. Heinig, T. Müller, B. Schmidt, M. Strobel, and W. Möller, "Interfaces under ion irradiation: Growth and taming of nanostructures," *Applied Physics A: Materials Science and Processing*, vol. 77, pp. 17–25, 2003.
- D. Q. Yang and E. Sacher, "Ar⁺-induced surface defects on HOPG and their effect on the nucleation, coalescence and growth of evaporated copper," *Surface Science*, vol. 516, pp. 43–55, 2002.
- D. Q. Yang, K. N. Piyakis, and E. Sacher, "The manipulation of Cu cluster dimensions on highly oriented pyrolytic graphite surfaces by low energy ion beam irradiation," *Surface Science*, vol. 536, pp. 67–74, 2003.
- F. Ruffino, R. De Bastiani, M. G. Grimaldi, C. Bongiorno, F. Giannazzo, F. Roccaforte, C. Spinella, and V. Raineri, "Self-organization of Au nanoclusters on the SiO₂ surface induced by 200 keV-Ar⁺ irradiation," *Nuclear Instruments and Methods in Physics Research, Section B: Beam Interactions with Materials and Atoms*, vol. 257, pp. 810–814, 2007.
- J. C. Love, L. A. Estroff, J. K. Kriebel, R. G. Nuzzo, and G. M. Whitesides, "Self-assembled monolayers of thiolates on metals as a form of nanotechnology," *Chemical reviews*, vol. 105, no. 4, pp. 1103–69, Apr. 2005. [Online]. Available: <http://www.ncbi.nlm.nih.gov/pubmed/15826011>
- B. O'Rourke, M. Flores, V. Esaulov, and Y. Yamazaki, "Modification of self assembled monolayers by highly charged ions," *Nuclear Instruments and Methods in Physics Research Section B: Beam Interactions with Materials and Atoms*, vol. 299, pp. 68–70, Mar. 2013. [Online]. Available: <http://linkinghub.elsevier.com/retrieve/pii/S0168583X13001845>
- B. Arezki, A. Delcorte, A. Chami, B. Garrison, and P. Bertrand, "Gold-thiolate cluster emission from SAMs under keV ion bombardment: Experiments and molecular dynamics simulations," *Nuclear Instruments and Methods in Physics Research Section B: Beam Interactions with Materials and Atoms*, vol. 212, pp. 369–375, Dec. 2003. [Online]. Available: <http://linkinghub.elsevier.com/retrieve/pii/S0168583X03014575>
- B. Arezki, A. Delcorte, B. J. Garrison, and P. Bertrand, "Understanding gold-thiolate cluster emission from self-assembled monolayers upon kiloelectronvolt ion bombardment," *The journal of physical chemistry. B*, vol. 110, no. 13, pp. 6832–40, Apr. 2006. [Online]. Available: <http://www.ncbi.nlm.nih.gov/pubmed/16570992>
- P. Cyganik, Z. Postawa, C. Meserole, E. Vandeweert, and N. Winograd, "Ion-induced erosion of organic self-assembled monolayers," *Nuclear Instruments and Methods in Physics Research Section B: Beam Interactions with Materials and Atoms*, vol. 148, no. 1-4, pp. 137–142, Jan. 1999. [Online]. Available: <http://linkinghub.elsevier.com/retrieve/pii/S0168583X98007514>
- C. Vericat, M. E. Vela, and R. C. Salvarezza, "Self-assembled monolayers of alkanethiols on Au(111): surface structures, defects and dynamics," *Physical chemistry chemical physics : PCCP*, vol. 7, no. 18, pp. 3258–68, Sep. 2005. [Online]. Available: <http://www.ncbi.nlm.nih.gov/pubmed/16240039>
- J. Pomeroy, A. Perrella, H. Grube, and J. Gillaspay, "Gold nanostructures created by highly charged ions," *Physical Review B*, vol. 75, no. 24, p. 241409, Jun. 2007. [Online]. Available: <http://link.aps.org/doi/10.1103/PhysRevB.75.241409>
- J. Pomeroy, H. Grube, A. Perrella, and J. Gillaspay, "STM and transport measurements of highly charged ion modified materials," *Nuclear Instruments and Methods in Physics Research Section B: Beam Interactions with Materials and Atoms*, vol. 258, no. 1, pp. 189–193, May 2007. [Online]. Available: <http://linkinghub.elsevier.com/retrieve/pii/S0168583X06013802>
- F. Aumayr, A. El-Said, and W. Meissl, "Nano-sized surface modifications induced by the impact of slow highly charged ions – A first review," *Nuclear Instruments and Methods in Physics Research Section B: Beam Interactions with Materials and Atoms*, vol. 266, no. 12-13, pp. 2729–2735, Jun. 2008. [Online]. Available: <http://linkinghub.elsevier.com/retrieve/pii/S0168583X08003765>
- L. Costelle, T. T. Jarvi, M. T. Raisanen, V. Tuboltsev, and J. Raisanen, "Binding of deposited gold clusters to thiol self-assembled monolayers on Au(111) surfaces," *Applied Physics Letters*, vol. 98, no. 4, p. 043107, 2011. [Online]. Available: <http://scitation.aip.org/content/aip/journal/apl/98/4/10.1063/1.3548862>
- L. Costelle, M. T. Raisanen, J. T. Joyce, C. Silien, L.-S. Johansson, J. M. Campbell, and J. Raisanen, "Structural Evolution of Gas-Phase Coinage Metal Clusters in Thiolate Self-Assembled Monolayers on Au," *The Journal of Physical Chemistry C*, vol. 116, no. 42, pp. 22602–22607, Oct. 2012. [Online]. Available: <http://pubs.acs.org/doi/abs/10.1021/jp307148p>
- "Sigma Aldrich." [Online]. Available: <http://www.sigmaaldrich.com/catalog/product/aldrich/471364>
- P. Klapetek, D. Necas, "Gwyddion," 2014. [Online]. Available: <http://gwyddion.net/>
- A. Rai, J. Nayak, and S. Roy Barman, "Temporal evolution and nature of nanostructures on Au(111)," *Surface Science*, vol. 625, pp. 97–103, Jul. 2014. [Online]. Available: <http://linkinghub.elsevier.com/retrieve/pii/S0039602814000703>
- M. H. Dishner, "Preparation of gold thin films by epitaxial growth on mica and the effect of flame annealing," *Journal of Vacuum Science & Technology A: Vacuum, Surfaces, and Films*, vol. 16, no. 6, p. 3295, Nov. 1998. [Online]. Available: <http://scitation.aip.org/content/avs/journal/jvsta/16/6/10.1116/1.581536>
- J. Barth, H. Brune, G. Ertl, and R. Behm, "Scanning tunneling microscopy observations on the reconstructed Au(111) surface: Atomic structure, long-range superstructure, rotational domains, and surface defects," *Physical Review B*, vol. 42, no. 15, pp. 9307–9318, Nov. 1990. [Online]. Available: <http://link.aps.org/doi/10.1103/PhysRevB.42.9307>
- A. C. Bose and M. Yoshitake, "Pattern formation induced by Ar⁺ sputtering on Au(111)," *Applied Surface Science*, vol. 241, no. 1-2, pp. 174–178, Feb. 2005. [Online]. Available: <http://linkinghub.elsevier.com/retrieve/pii/S016943320401387X>
- P. Maksymovych, D. C. Sorescu, and J. T. Yates, "Gold-atom-mediated bonding in self-assembled short-chain alkanethiolate species on the Au(111) surface," *Physical Review Letters*, vol. 97, no. 14, p. 146103, 2006.
- A. Oliva-Florio, R. Baragiola, M. Jakas, E. Alonso, and J. Ferrón, "Noble-gas ion sputtering yield of gold and copper: Dependence on

- the energy and angle of incidence of the projectiles," *Physical Review B*, vol. 35, no. 5, pp. 2198–2204, Feb. 1987. [Online]. Available: <http://link.aps.org/doi/10.1103/PhysRevB.35.2198>
- 28 A. Bondi, "van der Waals Volumes and Radii," *The Journal of Physical Chemistry*, vol. 68, no. 3, pp. 441–451, Mar. 1964. [Online]. Available: <http://pubs.acs.org/doi/abs/10.1021/j100785a001>
- 29 J. F. Ziegler, "SRIM." [Online]. Available: <http://www.srim.org/>
- 30 S. Tanuma, C. J. Powell, and D. R. Penn, "Calculations of electron inelastic mean free paths. II. Data for 27 elemental solids over the 50–2000 eV range," *Surface and Interface Analysis*, vol. 17, no. 13, pp. 911–926, 1991.
- 31 J.-P. Bucher, L. Santesson, and K. Kern, "Thermal Healing of Self-Assembled Organic Monolayers: Hexane- and Octadecanethiol on Au(111) and Ag(111)," *Langmuir*, vol. 10, no. 4, pp. 979–983, Apr. 1994. [Online]. Available: <http://pubs.acs.org/doi/abs/10.1021/la00016a001>
- 32 M. Flores, B. O'Rourke, Y. Yamazaki, and V. Esaulov, "Potential and kinetic sputtering of alkanethiol self-assembled monolayers by impact of highly charged ions," *Physical Review A*, vol. 79, no. 2, p. 022902, Feb. 2009. [Online]. Available: <http://link.aps.org/doi/10.1103/PhysRevA.79.022902>
- 33 M. Godin, P. J. Williams, V. Tabard-Cossa, O. Laroche, L. Y. Beaulieu, R. B. Lennox, and P. Grütter, "Surface stress, kinetics, and structure of alkanethiol self-assembled monolayers." *Langmuir : the ACS journal of surfaces and colloids*, vol. 20, no. 17, pp. 7090–6, Aug. 2004. [Online]. Available: <http://www.ncbi.nlm.nih.gov/pubmed/15301492>
- 34 A. P. Labonté, S. L. Tripp, R. Reifengerger, and A. Wei, "Scanning tunneling spectroscopy of insulating self-assembled monolayers on Au(111)," *Journal of Physical Chemistry B*, vol. 106, pp. 8721–8725, 2002.
- 35 C. Vericat, M. E. Vela, G. Benitez, P. Carro, and R. C. Salvarezza, "Self-assembled monolayers of thiols and dithiols on gold: new challenges for a well-known system." *Chemical Society reviews*, vol. 39, no. 5, pp. 1805–34, May 2010. [Online]. Available: <http://www.ncbi.nlm.nih.gov/pubmed/20419220>
- 36 M. M. Biener, J. Biener, and C. M. Friend, "Revisiting the S-Au(111) interaction: Static or dynamic?" *Langmuir*, vol. 21, no. 111, pp. 1668–1671, 2005.
- 37 F. Chesneau, J. Zhao, C. Shen, M. Buck, and M. Zharnikov, "Adsorption of Long-Chain Alkanethiols on Au(111): A Look from the Substrate by High Resolution X-ray Photoelectron Spectroscopy," *The Journal of Physical Chemistry C*, vol. 114, no. 15, pp. 7112–7119, Apr. 2010. [Online]. Available: <http://pubs.acs.org/doi/abs/10.1021/jp100522n>
- 38 T. Weidner, N. Ballav, U. Siemeling, D. Troegel, T. Walter, R. Tacke, D. G. Castner, and M. Zharnikov, "Tripodal Binding Units for Self-Assembled Monolayers on Gold: A Comparison of Thiol and Thioether Headgroups." *The journal of physical chemistry. C, Nanomaterials and interfaces*, vol. 113, no. 45, pp. 19 609–19 617, Nov. 2009. [Online]. Available: <http://www.pubmedcentral.nih.gov/articlerender.fcgi?artid=3102536&tool=pmcentrez&rendertype=abstract>
- 39 M. Himmelhaus, I. Gauss, M. Buck, F. Eisert, C. Wöll, and M. Grunze, "Adsorption of docosanethiol from solution on polycrystalline silver surfaces: an XPS and NEXAFS study," *Journal of Electron Spectroscopy and Related Phenomena*, vol. 92, no. 1-3, pp. 139–149, May 1998. [Online]. Available: <http://linkinghub.elsevier.com/retrieve/pii/S0368204898001157>
- 40 T. Ishida, W. Mizutani, U. Akiba, K. Umemura, A. Inoue, N. Choi, M. Fujihira, and H. Tokumoto, "Lateral Electrical Conduction in Organic Monolayer," *The Journal of Physical Chemistry B*, vol. 103, no. 10, pp. 1686–1690, Mar. 1999. [Online]. Available: <http://pubs.acs.org/doi/abs/10.1021/jp983547x>
- 41 Y. Yang and L. Fan, "High-Resolution XPS Study of Decanethiol on Au(111): Single Sulfur-Gold Bonding Interaction." *Langmuir*, vol. 18, no. 4, pp. 1157–1164, Feb. 2002. [Online]. Available: <http://pubs.acs.org/cgi-bin/doilookup?10.1021/la010591m>
- 42 K. S. S. Liu, C. W. Yong, B. J. Garrison, and J. C. Vickerman, "Molecular Dynamics Simulations of Particle Bombardment Induced Desorption Processes: Alkanethiolates on Au(111)," *The Journal of Physical Chemistry B*, vol. 103, no. 16, pp. 3195–3205, Apr. 1999. [Online]. Available: <http://pubs.acs.org/doi/abs/10.1021/jp984071k>
- 43 T. Laiho, J. Leiro, and J. Lukkari, "XPS study of irradiation damage and different metal-sulfur bonds in dodecanethiol monolayers on gold and platinum surfaces," *Applied Surface Science*, vol. 212-213, pp. 525–529, May 2003. [Online]. Available: <http://linkinghub.elsevier.com/retrieve/pii/S0169433203004628>
- 44 T. M. Willey, A. L. Vance, T. van Buuren, C. Bostedt, L. Terminello, and C. Fadley, "Rapid degradation of alkanethiol-based self-assembled monolayers on gold in ambient laboratory conditions," *Surface Science*, vol. 576, no. 1-3, pp. 188–196, Feb. 2005. [Online]. Available: <http://linkinghub.elsevier.com/retrieve/pii/S0039602804015535>
- 45 A. Ulman, "Formation and Structure of Self-Assembled Monolayers." *Chemical reviews*, vol. 96, no. 4, pp. 1533–1554, Jun. 1996. [Online]. Available: <http://www.ncbi.nlm.nih.gov/pubmed/11848802>